JOURNAL OF GUIDANCE, CONTROL, AND DYNAMICS
Vol. 19, No. 5, September–October 1996

Ground-Based Simulation of Space Manipulators Using Test Bed with Suspension System

Hironori A. Fujii,* Kenji Uchiyama,† and Hideharu Yoneoka‡
Tokyo Metropolitan Institute of Technology, Hino, Tokyo 191, Japan
and
Tsugito Maruyama§
Fujitsu Laboratories, Ltd., Nakaharaku, Kawasaki 211, Japan

An experimental system simulating dynamic behavior of space manipulators is constructed for the purpose of technological demonstration of space robots and evaluation of their dynamic features. The system consists of a space robot with dual manipulators, a suspension system, and a control system. The manipulators are hung by wires at each joint of the manipulators to cancel the effect of the ground gravitational force. The tension of the wires is controlled to be constant to simulate on the ground the dynamic behavior of the manipulators in space. Dynamics of the two-link manipulators is analyzed experimentally employing the present ground facility through inspection of their dynamic features in space. The motion of the manipulator is restricted to a vertical plane as the first step of study. The outline of the experimental system is also briefly introduced. The results of the numerical simulation and the experiments show sufficient capability of the on-ground simulation to study dynamic behavior of the manipulator in space.

I. Introduction

CURRENT plans and future vision for space development include such tasks as assembling and maintaining space structures and a variety of infrastructures. Space manipulator systems have increased in importance for space development in proportion to the growth of complexity of space missions.

Numerical and experimental simulations of space manipulator systems on the ground are necessary and important to predict dynamic behavior of the manipulators in space. Differences exist in dynamic features on the ground and in space because of environmental features, e.g., the gravity condition. Despite the difficulty of simulating space environments such as microgravity conditions, numerical simulations and experiments conducted on the ground are necessary to exploit the dynamics of space manipulator systems.

Research[1–14] on space robots has been reported describing several methods to simulate on the ground the dynamics of robots in space, which are devoted to studying important problems inherent in the ground tests. The following methods of gravity compensation are available for this purpose: 1) fly the model freely in a horizontal plane by using air cushion or air bearings; 2) cancel the gravitational force with use of water buoyancy in a pool; 3) undertake experiments in an airplane flying along a parabolic trajectory, or use free-falling capsule on the ground facility; 4) hang the experimental model by wires canceling the gravitational force by tension of the wires at selected points; and 5) estimate the dynamic behavior of a space robot through numerical processing in a mathematical model.

Among them, methods 1–4 are mechanical methods and are the concern of the present study. Experiments on dynamics and control of the manipulator are reported by employing method 1 (Refs. 6–9). Method 1 has a drawback that motion of the manipulator is restricted to a planar motion. Demonstration of space robot dynamics is difficult using method 2 because its motion is influenced by the water resistance. Method 3 is not appropriate to simulate such dynamics since the laboratory space and the time for the experiment are limited. A few studies have been reported that employ method 4 (Refs. 12–14). This paper treats method 4, which has the ability to simulate dynamic behavior of the manipulator in three-dimensional motion, having no predominant force such as fluid drag as in method 2, and no constraint such as the limited short period of time of method 3.

A sufficient performance to control the tension of wire is necessary to simulate the microgravity condition on the ground using method 4. The manipulators are hung by wires at each joint while the values of tension of wires are constantly controlled to cancel the gravitational force acting on the manipulators. Such control of the tension of wires for the case of the flexible manipulator is also assessed for future study in this paper.

II. Control of Wire Tension for Microgravity Condition

In this section, we derive the equations of motion of a manipulator system and study a control method of tension of wires to simulate the microgravity condition on the ground. Figure 1 shows a schematic representation of the system model for ground simulation of the dynamic behavior of a space manipulator when its joints are suspended by wires. The flexibility on the link of the manipulator is considered to clarify the possibility of the gravity compensation with a suspension system. The coordinate system is referred to as the virtual link coordinate system[15] since the boundary conditions of the system are simply represented.

The following assumptions are made for the analysis.

1) The flexible link of the manipulator is the Euler–Bernoulli beam for which rotary inertia and shear deformation effects are ignored.

2) The bending rigidity and line density of the each link are constant along the link.

3) Nonlinear features such as the friction and backlash in the motor dynamics are neglected.

The manipulator is actuated to rotate in the inertial space by the torque τ_i of the motor, which is assumed to be a particle with mass m_i placed at the joints of the manipulator. Every joint of the manipulator is suspended by wires vertically to cancel the effect of the gravitational force. In Fig. 1, the orthogonal axes x and y denote the inertial coordinate system and the parameters $u_i (i = 1, \ldots, n)$

Received March 4, 1994; revision received Jan. 29, 1996; accepted for publication Feb. 22, 1996.

*Professor, Department of Aerospace Engineering. Associate Fellow AIAA.

†Graduate Student, Department of Aerospace Engineering; currently Research Associate, Department of Precision Engineering, Tokyo Metropolitan University, Hachiokji, Tokyo 192-03, Japan. Student Member AIAA.

‡Graduate Student, Department of Aerospace Engineering; currently Researcher, Riso Kagaku Co., Minato-Ku, Tokyo 108, Japan.

§Senior Researcher, Space System Laboratory, Multimedia System Laboratories.

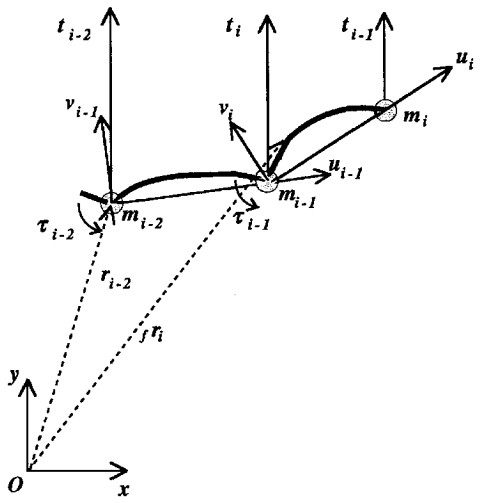

Fig. 1 Schematic representation of the system model.

are set along the link from the origin at the $(i-1)$th coordinate system to origin at the ith coordinate system.

The position vector of the ith joint of the manipulator from the origin of the inertial coordinate system O to the ith motor attached at the joint of the manipulator is defined as

$$\boldsymbol{r}_i = \boldsymbol{r}_0 + \sum_{j=1}^{i} \boldsymbol{l}_j \tag{1}$$

$$\boldsymbol{r}_0 = x\boldsymbol{e}_x + y\boldsymbol{e}_y \tag{2}$$

$$\boldsymbol{l}_i = l_i \boldsymbol{e}_{u_i} \tag{3}$$

where $\boldsymbol{r}_0$ and $\boldsymbol{l}_i$ denote the position vector of the base of the manipulator from the origin O and the position vector from the $(i-1)$th joint to ith joint of the manipulator $(i = 1, \ldots, n)$. The parameters $\boldsymbol{e}_x$, $\boldsymbol{e}_y$, and $\boldsymbol{e}_{u_i}$ denote the unit vectors corresponding to the inertia coordinates x, y, and the rotational coordinate u_i, respectively, as shown in Fig. 1. The position vector $\boldsymbol{r}_i$ represented in Eq. (1) can be rewritten as the following equation by using the direction cosine matrix:

$$\boldsymbol{r}_i = \boldsymbol{r}_0 + \sum_{j=1}^{i} \boldsymbol{R}_{\theta_j} \boldsymbol{l}_j \tag{4}$$

where

$$\boldsymbol{R}_{\theta_j} = \begin{bmatrix} \cos(\theta_1 + \cdots + \theta_j) & -\sin(\theta_1 + \cdots + \theta_j) \\ \sin(\theta_1 + \cdots + \theta_j) & \cos(\theta_1 + \cdots + \theta_j) \end{bmatrix} \qquad j = 1, \ldots, n \tag{5}$$

The position vector of the ith flexible link of the manipulator from origin O to any element on the ith link by using Eq. (5) is denoted as

$$_f\boldsymbol{r}_i = \boldsymbol{r}_{i-1} + \boldsymbol{R}_{\theta_i} \cdot {}_f\boldsymbol{l}_i \tag{6}$$

$$_f\boldsymbol{l}_i = u_i \boldsymbol{e}_{u_i} + v_i \boldsymbol{e}_{v_i} \tag{7}$$

where $_f\boldsymbol{l}_i$ denotes the position vector $(i-1)$th joint of the manipulator to the element of the ith link of the manipulator.

The kinetic energy K of the manipulator system is represented as

$$\begin{aligned} K &= \sum_{i=0}^{n} k_i \\ &= \sum_{i=0}^{n} \left(\frac{1}{2} m_i \dot{\boldsymbol{r}}_i \cdot \dot{\boldsymbol{r}}_i + \frac{1}{2} \int_0^{l_i} \rho_i \, {}_f\dot{\boldsymbol{r}}_i \cdot {}_f\dot{\boldsymbol{r}}_i \, \mathrm{d}u_i \right) \\ &= \sum_{i=0}^{n} \left({}_m k_i + \int_0^{l_i} {}_e k_i \, \mathrm{d}u_i \right) \end{aligned} \tag{8}$$

where the position vectors $\boldsymbol{r}_i$ and $_f\boldsymbol{r}_i$ are functions of coordinates x, y, and $\theta_i (i = 1, \ldots, n)$ and the parameters $\rho_i (i = 1, \ldots, n)$ denote the line density of the ith link of the manipulator. The time derivatives of the position vectors $\boldsymbol{r}_i$ and $_f\boldsymbol{r}_i$ can be easily obtained from Eqs. (1) and (6). The first and second terms on the right-hand side of Eq. (8) denote the kinetic energy corresponding to the ith rigid body and the kinetic energy corresponding to ith flexible link, respectively.

The potential energy of the manipulator system is constant with respect to the coordinates x, y, and $\theta_i (i = 1, \ldots, n)$ if the system is constrained in zero-gravity environments or a horizontal plane. However, the potential energy of the present manipulator system arises from the gravitational force and elastic deformation of the link of the manipulator and is defined as

$$\begin{aligned} P &= \sum_{i=0}^{n} p_i \\ &= \sum_{i=0}^{n} \left(m_i g \left[y + \sum_{j=0}^{i} l_i \sin\left(\sum_{k=0}^{j} \theta_k \right) \right] \right. \\ &\quad + \int_0^{l_i} \left\{ \frac{1}{2} E I_i \left(\frac{\partial^2 v_i}{\partial u_i^2} \right) + \rho_i l_i g \left[y + \sum_{j=0}^{i} l_i \sin\left(\sum_{k=0}^{j} \theta_k \right) \right] \right. \\ &\quad \left. \left. + u_i \sin\left(\sum_{j=0}^{i} \theta_j \right) + v_i \cos\left(\sum_{j=0}^{i} \theta_j \right) \right\} \mathrm{d}u_i \right) \\ &= \sum_{i=0}^{n} \left({}_m p_i + \int_0^{l_i} {}_e p_i \, \mathrm{d}u_i \right) \end{aligned} \tag{9}$$

where $EI_i (i = 1, \ldots, n)$ is the bending rigidity of the ith link of the manipulator. The first term of the right-hand side in Eq. (9) denotes the potential energy corresponding to ith joint, and the second term the potential energy corresponding to ith link.

The work W done by the torque τ_i and the tension t_i is given as follows:

$$\begin{aligned} W = \sum_{i=0}^{n} \left\{ \tau_i \left(\theta_{i+1} + \frac{\partial v_{i+1}}{\partial u} \bigg|_{u_{i+1}=0} - \frac{\partial v_{i+1}}{\partial u} \bigg|_{u_i = l_i} \right) \right. \\ \left. + t_i \left[y_i + \sum_{j=1}^{i} l_i \sin\left(\sum_{k=1}^{j} \theta_k \right) \right] \right\} \end{aligned} \tag{10}$$

where $y_i (i = 0, \ldots, n)$ is the displacement at the ith joint of the manipulator caused by the wire tension t_i. As already mentioned, the friction and backlash in the torque motor attached at each joint of the manipulator are neglected in the analysis of the motion of the manipulator system.

Using Hamilton's principle,[16] the equations of motion are obtained from Eqs. (8–10) as follows:

$$\frac{\mathrm{d}}{\mathrm{d}t} \left(\frac{\partial K}{\partial \dot{x}} \right) = 0 \tag{11a}$$

$$\frac{\mathrm{d}}{\mathrm{d}t} \left(\frac{\partial K}{\partial \dot{y}} \right) + \frac{\partial P}{\partial y} - \sum_{i=0}^{n} t_i = 0 \tag{11b}$$

$$\begin{aligned} \sum_{j=1}^{n+1-i} \left\{ \frac{\mathrm{d}}{\mathrm{d}t} \left(\frac{\partial K}{\partial \dot{\theta}_i} \right) - \frac{\partial}{\partial \theta_i} (k_{n+1-j} - p_{n+1-j}) \right. \\ \left. - t_{n+1-j} \left[\sum_{k=j}^{n+1-i} l_{n+1-k} \cos\left(\sum_{l=1}^{n+i-k} \theta_i \right) \right] \right\} = \tau_i \end{aligned} \tag{11c}$$

$$\frac{\mathrm{d}}{\mathrm{d}t} \left(\frac{\partial {}_e k_i}{\partial \dot{v}_i} \right) - \frac{\partial}{\partial v_i} ({}_e k_i - {}_e p_i) + \frac{\partial^2}{\partial u_i^2} \left(\frac{\partial {}_e p_i}{\partial v_i''} \right) = 0 \tag{11d}$$

where

$$v_i'' = \frac{\partial^2 v_i}{\partial u_i^2} \tag{12}$$

Equations (11a) and (11b) represent the motion of the system model corresponding to the x and y coordinates, respectively, of the inertial coordinate system, as shown in Fig. 1. Note that Eq. (11a) represents the conservation of the momentum corresponding to the coordinate x. The second term on the left-hand side of Eq. (11b) denotes the gravitational term, and third term in Eq. (11b) is the tension term. If the tension term is equal to the gravitational term, Eq. (11b) can be treated as the equation of motion of manipulators in space. Equation (11c) gives the expression for the ith torque at the actuators of the manipulator as a function of joint position, velocity, and acceleration. The motion of the lateral vibration of the ith link is represented in Eq. (11d).

The boundary conditions of the present space manipulator system are

$$\tau_{i-1} + \left.\frac{\partial_e p_i}{\partial v_i''}\right|_{u_i=0} = 0 \tag{13a}$$

$$\tau_i + \left.\frac{\partial_e p_i}{\partial v_i''}\right|_{u_i=l_i} = 0 \tag{13b}$$

$$v_i|_{u_i=0} = v_i|_{u_i=l_i} = 0 \tag{13c}$$

From inspection of Eqs. (11b) and (11c), the values of tension are obtained to simulate the space environment microgravity condition on the ground as follows:

$$\frac{\partial p}{\partial y} - \sum_{i=0}^{n} t_i = 0 \tag{14a}$$

$$\sum_{j=1}^{n+1-i}\left\{\frac{\partial}{\partial\theta_i}(p_{n+1-j}) - t_{n+1-j} \times\left[\sum_{k=j}^{n+1-j} l_{n+1-k}\cos\left(\sum_{l=1}^{n+i-k}\theta_l\right)\right]\right\} = 0 \tag{14b}$$

Both Eqs. (14a) and (14b) show the possibility for simulating on the ground the dynamic behavior of the space manipulator in space when the model of the link can be assumed to be rigid. If the link is flexible, it is seen to be difficult to completely simulate on the ground the lateral vibration because of the lack of the force to cancel the gravitational force acting on the link of the space manipulator as shown in Eq. (11d).

III. Description of Experimental System

A. Mechanical Configuration

The experimental system for the space robot employs a suspension system to simulate microgravity conditions on the ground. A photograph of the experimental device is shown in Fig. 2. The system consists of a model of a space robot with dual manipulators, a suspension system, and a control system. The manipulators are

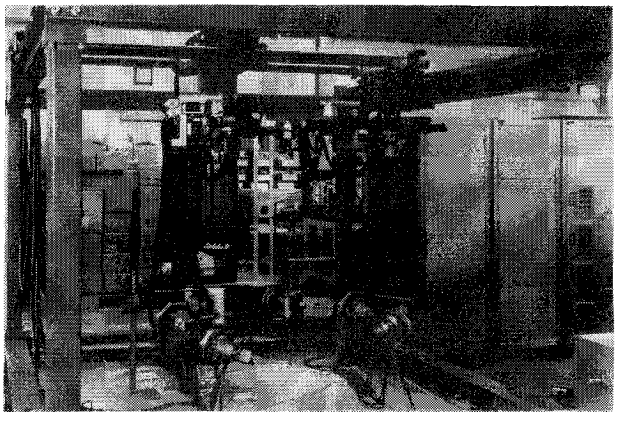

Fig. 2 Photograph of the experimental device for space robot using suspension system.

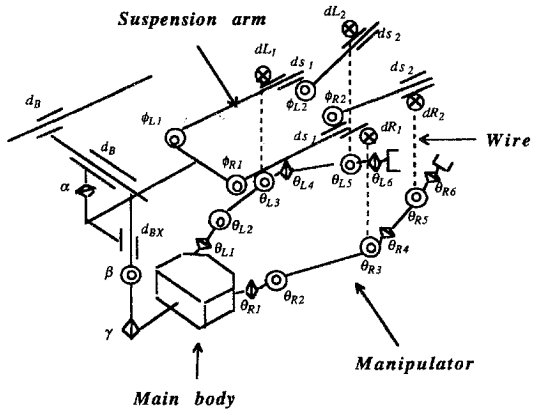

Fig. 3 System DOFs on the experimental device for space robot.

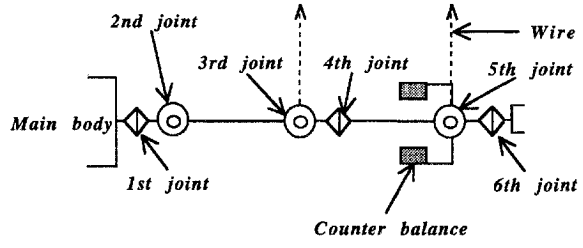

Fig. 4 Construction of the manipulator of space robot.

hung by wires at each joint to cancel the effect of gravitational force acting on them. The system degrees of freedom (DOFs) of the space robot and the suspension system are shown in Fig. 3.

The base of the space robot has six DOFs (three DOFs for translational motion and three DOFs for rotational motion). The free-flying motion of the main body of the space robot is simulated based on the numerical integration of the dynamic equations for the manipulators. The model of the space robot consists of the main body and the dual manipulators possessing three links per arm with six DOFs for each. Direct drive (DD) motors are equipped to actuate the manipulators of the space robot and are not powerful enough to actuate the manipulators on the 1-g condition in comparison with a geared motor because of the lack of a gear reducer in its structure. The DD motors have enough power to actuate the manipulator in space. Furthermore, there are many advantages in using the DD motor, e.g., the backlash and the friction are negligible, and no lubricating oil is necessary in the space environment of a vacuum. Each arm of the manipulator is 1.4 m long and weighs 25 kg; the DD motors need the help of the suspension wires to support the total weight of the arm on the ground. The wires are connected to gimbal joints, which enable smooth rotation of the arm around all three orthogonal axes.

The suspension arms have four DOFs for each arm, and their motion is restricted to the horizontal plane to avoid complicating the mechanisms. Two wires are used to suspend the manipulators for each arm. In view of the simplification of the mechanism, counterbalance weights are attached to the fifth joint to balance the weight of the third link, as shown in Fig. 4. The tip arm consists of a third link and counterbalance, and the center of the mass of the tip arm is located to be precisely on the fifth joint.

B. Suspension System

The suspension system consists of two suspension arms and four tension sensors. As discussed in Sec. II, the value of the tension of wires must be controlled to remain constant to simulate the dynamic behavior of space manipulators. In fact, keeping the tension of the wires constant when the space manipulator moves is not sufficient to simulate exactly the microgravity environment. The friction at the pulleys in the tension control system introduces a problem, which disturbs the smooth motion of the space manipulator. Therefore, a control scheme is employed to achieve both constant tension control and friction compensation.[14] In the process of tension control, the tension strength is directly sensed through a tension sensor, as shown

in Fig. 5. The triangularly arranged pulleys transform the vertical component force of the wire tension into a horizontal component force, sensed through strain gauges attached to the plate spring. The tension sensor is shown to be reliable for the range of tension strength less than 15 kg, where the proportional relation between tension strength and output of the strain gauges is quite satisfactory.

The suspension arm must be maneuvered to follow the motion of the manipulator, keeping the hanging wire vertical and then simulating the microgravity environment in both the horizontal and vertical directions. The coordinate system of the suspension arm is shown in Fig. 6. The points d_{L1} and d_{L2} in Fig. 6 correspond to the suspending points on the suspension arms. The position of the third joint from the origin of coordinates system of base Σ_s is obtained as

$$\begin{bmatrix} Y_{s1} \\ Z_{s1} \end{bmatrix} = \begin{bmatrix} -C_{sL2} - d_{sL1}s\phi_{L1} - C_{sL3}c\phi_{L1} \\ C_{s1} + d_{sL1}c\phi_{L1} - C_{sL3}s\phi_{L1} \end{bmatrix} \tag{15}$$

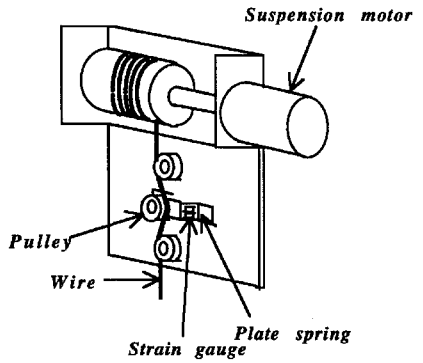

Fig. 5 Tension sensor.

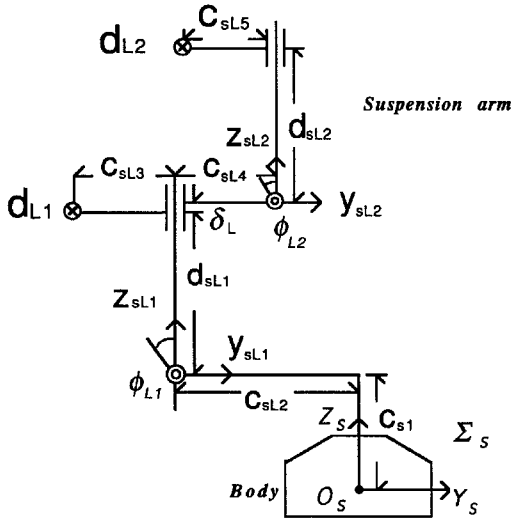

Fig. 6 Coordinates of suspension arm.

where $c\phi_{L1} = \cos\phi_{L1}$ and $s\phi_{L1} = \sin\phi_{L1}$. Using Eq. (15), ϕ_{L1} and d_{sL1} are obtained as follows:

$$\phi_{L1} = \sin^{-1}\left(\frac{-C_{sL3}}{\sqrt{y_1^2 + z_1^2}}\right) - \sin^{-1}\left(\frac{y_1}{\sqrt{y_1^2 + z_1^2}}\right) \tag{16}$$

$$d_{sL1} = \sqrt{y_1^2 + z_1^2 - C_{sL3}^2} \tag{17}$$

where

$$y_1 = Y_{s1} + C_{sL2} \tag{18}$$

$$z_1 = Z_{s1} - C_{s1} \tag{19}$$

Similarly, the position of the fifth joint from the origin of coordinates of base Σ_s is obtained as follows:

$$\begin{bmatrix} Y_{s2} \\ Z_{s2} \end{bmatrix} = \begin{bmatrix} -C_{sL2} - d_{sL}s\phi_{L1} + C_{sL4}c\phi_{L1} - d_{sL2}s\phi_{L2} - C_{sL5}s\phi_{L2} \\ C_{sL2} + d_{sL}c\phi_{L1} + C_{sL4}s\phi_{L1} + d_{sL2}c\phi_{L2} + C_{sL5}c\phi_{L2} \end{bmatrix} \tag{20}$$

where

$$d_{sL} = d_{sL1} + \delta_L \tag{21}$$

$$\phi_{12} = \phi_{L1} + \phi_{L2} \tag{22}$$

Using Eq. (20), ϕ_{L2} and d_{sL2} are obtained as follows:

$$\phi_{L2} = \sin^{-1}\left(\frac{-C_{sL5}}{\sqrt{y_2^2 + z_2^2}}\right) - \sin^{-1}\left(\frac{y_2}{\sqrt{y_2^2 + z_2^2}}\right) - \phi_{L1} \tag{23}$$

$$d_{sL2} = \sqrt{y_2^2 + z_2^2 - C_{sL5}^2} \tag{24}$$

where

$$y_2 = Y_{s2} + C_{sL2} + (d_{sL1} + \delta_L)s\phi_{L1} - C_{sL4}c\phi_{L1} \tag{25}$$

$$z_2 = Z_{s2} - C_{s1} - (d_{sL1} + \delta_L)c\phi_{L1} - C_{sL4}s\phi_{L1} \tag{26}$$

The suspension arms are controlled to keep the wire vertical through use of Eqs. (16), (17), (23), and (24).

C. Control System

Figure 7 shows the block diagram of the control system in the present experimental facility. The system consists of two digital computers (Fujitsu FMR-70HX3, 80386 + 387), three Digital Signal Processors (DSP) (Fujitsu DSP MB 8764), D/A converter, and tension control circuits.

The actuators of the suspension system and the space manipulator are controlled through the DSP and D/A converter, respectively. The

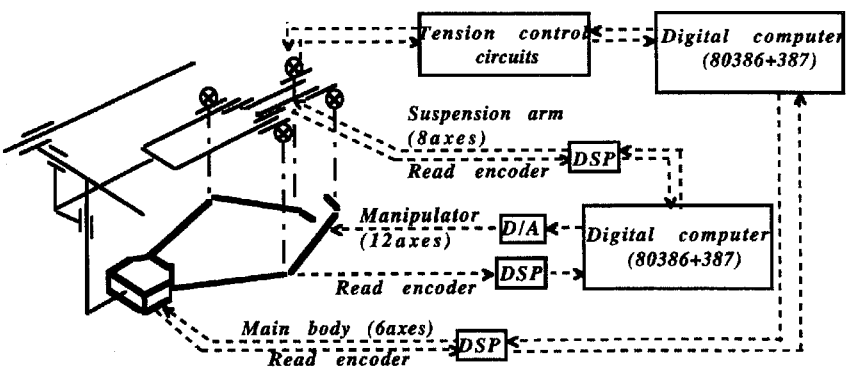

Fig. 7 Block diagram of the experimental system.

tension control system is directly implemented in analog control circuits, which are attached to a digital computer. Data from the DSP are put into a digital computer to process the value of the position, velocity, acceleration of the suspension arm, which are solutions of inverse kinematics. These data provide the operational path for the suspension arm in terms of the translational joint and the rotational joint time series. Motion of the manipulator in space is thus completely simulated on the ground. The sampling time in the present experiment is 10 ms.

IV. Experimental Results

The dynamic behavior of the two-link manipulator with fixed-base is analyzed through the experiments to evaluate the capability of the present experimental device. Figure 8 shows a schematic representation of the model treated in this paper. The model has two DOFs. The manipulator is assumed to move in the vertical plane for the first step of the analysis. The dynamic equations of the two-link manipulator including the effect of gravitational force can be described as follows:

$$M(\theta)\ddot{\theta} + d(\theta, \dot{\theta}) + h(\theta) = \tau + N(\theta)t \tag{27}$$

where the matrix $M(\theta) \in R^{2\times 2}$ is an inertial matrix of the manipulator. We denote angles of joint 1 and 2 as $\theta = (\theta_1 \ \theta_2)^T$ and the corresponding joint torque as $\tau = (\tau_1 \ \tau_2)^T$, and the tension of the wires connected at the joints of the manipulator as $t = (t_1 \ t_2)^T$. The superscript T indicates the transpose of the vector and matrix. The second term, $d(\theta, \dot{\theta}) \in R^{2\times 1}$, and the third term, $h(\theta) \in R^{2\times 1}$, on the left-hand side of Eq. (27) denote the column vector with respect to Coriolis and centrifugal force and the column vector with respect to the gravitational force, respectively.

From inspection on Eq. (27), the tension of the wires connected at each joint of the manipulator is seen to be necessary to satisfy the following equation to simulate the microgravity condition on the ground:

$$N(\theta)t - h(\theta) = 0 \tag{28}$$

where

$$N(\theta) = \begin{bmatrix} l_1 \cos\theta_1 & l_1 \cos\theta_1 + l_2 \cos(\theta_1 + \theta_2) \\ 0 & l_2 \cos(\theta_1 + \theta_2) \end{bmatrix} \tag{29}$$

The lengths of the links of the manipulator, l_1 and l_2, are defined as shown in Fig. 8. The tension of the wires, t_1 and t_2, can be obtained from Eq. (28) as in the following equations except for the case where the determinant of the matrix N is equal to zero, i.e., $\theta_1 + \theta_2 = \pi/2$ or $\theta_1 = \pi/2$:

$$t = \begin{bmatrix} t_1 \\ t_2 \end{bmatrix} = \begin{bmatrix} \left(m_1 + \frac{m_{l1}}{2} + \frac{m_{l2}}{2}\right)g \\ \left(m_2 + \frac{m_{l2}}{2}\right)g \end{bmatrix} \tag{30}$$

The parameters m_{l1} and m_{l2} on the right-hand side of Eq. (30) denote the mass of the first and the second link of the manipulator, respectively. Note that the wires are vertically connected to the joints of the manipulator and the tension of the wire has to be controlled as a constant value to cancel the gravitational force completely.

Figure 9 shows the time responses of the angles of the two-link manipulator whose motion is restricted in the vertical plane. The torque τ for the motors is only given at the second joint τ_2 in the form of bang-bang control. The dotted and solid lines denote the results of the numerical simulation and the experiment, respectively. Good agreement is seen between the results of the numerical simulation and the experiment in Fig. 9. The angle θ_1 of the first link is seen to reach -0.32 (rad) within 2.0 s in the numerical simulation and reaches -0.38 (rad) in the experiment. For angle θ_1, the maximum error between the numerical simulation and the experiment is 0.06 (rad) at the end of the experiment. Similarly, the angle of the second link, θ_2, is seen to reach about 0.78 (rad) in the results of the numerical simulation and the experiment.

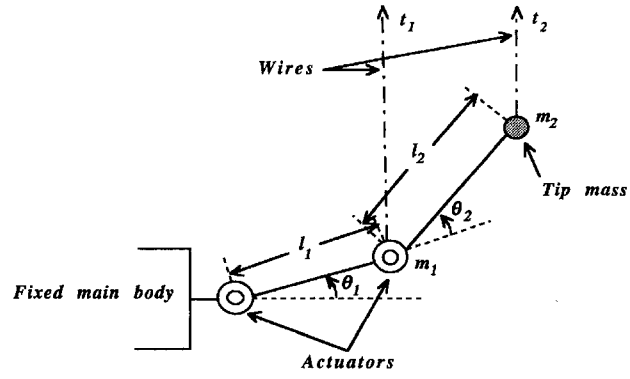

Fig. 8 Schematic representation of two-link manipulator.

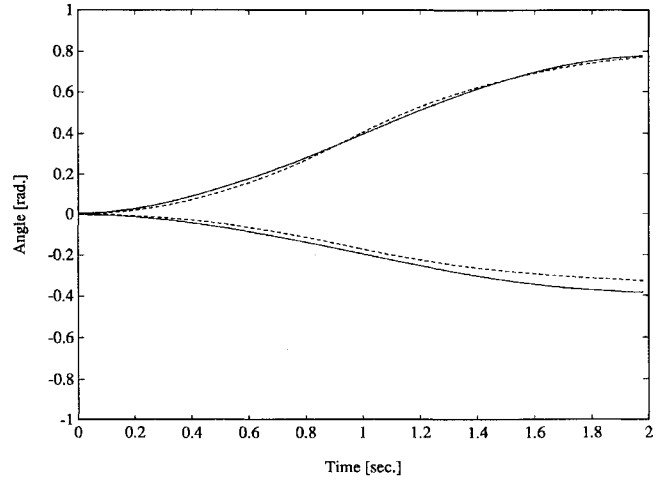

Fig. 9 Time history of the angle of the manipulator: ----, numerical simulation and ——, experiment.

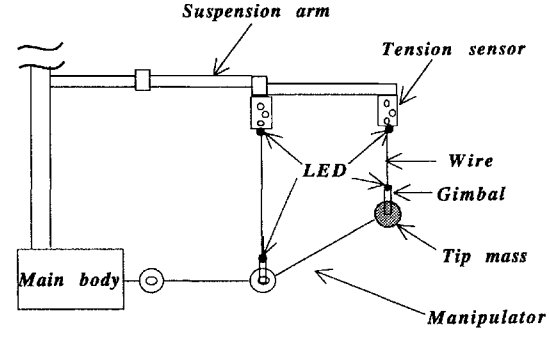

Fig. 10 Location of LED on the experimental device.

It is important to confirm that the suspending wires are maintained to be vertical to simulate the microgravity condition while the manipulator is moving in the vertical plane. The following two methods are used to evaluate the verticality of the wires: 1) compare the calculated data of the angle of the suspension arm with the measured data sensed by the encoder of the motors built in the suspension arm and 2) measure the inclination of the wires from the vertical line using the position sensor.

In method 1, the position of the suspension arms is defined geometrically to keep the wire vertical and can be calculated through use of the data on the angle of the manipulator. A position sensor (Video Trucker system) is employed to evaluate the vertical position of the suspending wires and four light emitting diodes are attached to the line of wires to be traced in the method 2, as shown in Fig. 10. Figure 11 shows the results of the evaluation of the wire verticality obtained from the first method. Figure 11a shows the results of the errors between the calculated data and measured data concerning the

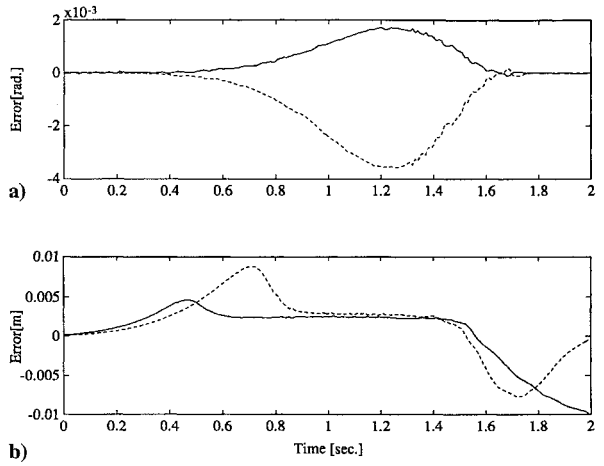

Fig. 11 Motion of the suspension arm: a) rotational joint: ----, first joint ϕ_{L1} and ——, second joint ϕ_{L2}; and b) prismatic joint: ----, first joint d_{sL1} and ——, second joint d_{sL2}.

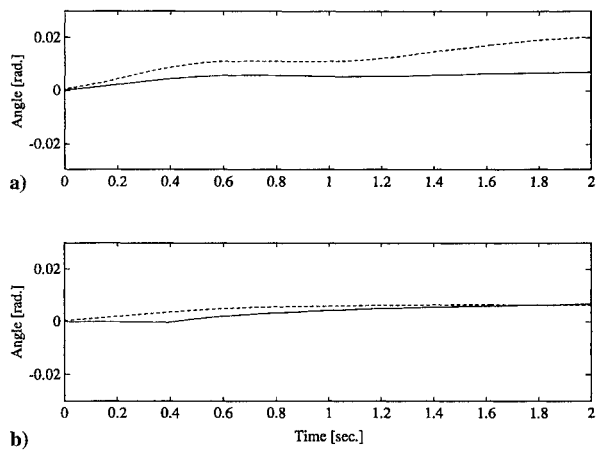

Fig. 12 Inclination of the wires: ----, wire connected at tip of manipulator and ——, wire connected at second joint of manipulator: a) front view of manipulator; and b) side view of manipulator.

rotational joint of the suspension arms. The broken and solid lines denote the error on the first rotational joint ϕ_{L1} and the error on the second rotational joint ϕ_{L2}, respectively, and the maximum error on the rotational joint is 5.5×10^{-3} rad. The errors on the prismatic joint of the suspension arms are shown in Fig. 11b. The broken and solid lines denote the error on the first prismatic joint d_{sL1} and the error on the second prismatic joint d_{sL2}, respectively, and the maximum error is 9.0×10^{-3} m. These results show that the suspension arms are well controlled to keep the wire vertical through the experiment. Figure 12 shows the wire angle while the manipulator is moving in the vertical plane, and the results for the inclination of wires from their vertical line are illustrated. Figures 12a and 12b show the wire angle from side view of the manipulator and from front view of the manipulator, respectively. The broken and solid lines denote the inclination of the wire connected at the tip of the manipulator and the inclination of the wire connected at the second joint of the manipulator, respectively. Note that the inclination of the wire is very small and the effect of the gravitational force caused by the inclination of the wire is shown to be negligible. The time responses of the tension of the wires are shown in Fig. 13. Figures 13a and 13b show the tension of the wires connected at the tip of the manipulator and the tension of the wires connected at the second joint of the manipulator. These values in Fig. 13 represent the variation in the tension from the equilibrium values. Figure 14 shows the experimental result of the tension of the wires in frequency domain. The natural frequency of the suspension system is seen to be 7.8 Hz, as shown in Fig. 14.

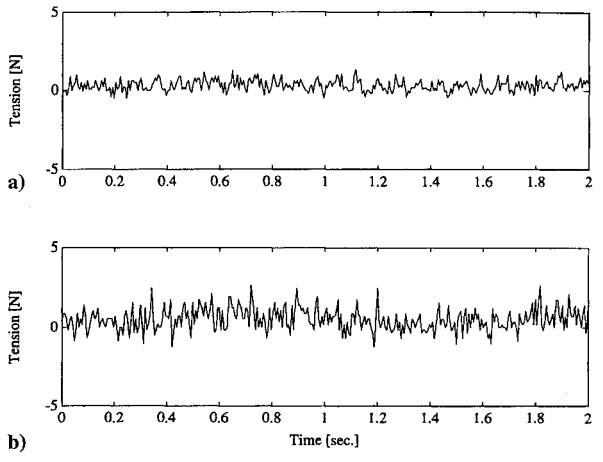

Fig. 13 Tension of wire: a) connected at tip of manipulator; and b) connected at second joint of manipulator.

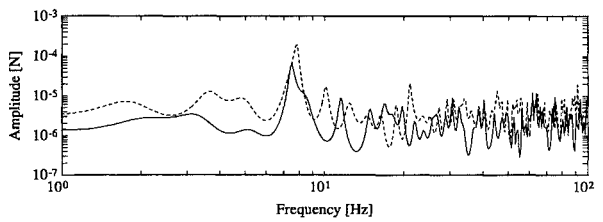

Fig. 14 Tension of wire in frequency domain: ----, wire connected at tip of manipulator and ——, wire connected at second joint of manipulator.

V. Conclusions

A method to actively compensate gravitational force is presented and analyzed to simulate experimentally the dynamics of a space manipulator on the ground. The manipulator is hung vertically through the wires on the ground to cancel the gravitational force, and the space environment microgravity condition is simulated.

The wires suspending the manipulator must be controlled to be vertical to simulate the microgravity condition. From results of the experiment, the effect of the gravitational force caused by the inclination of wires is shown to be negligible for the present experimental device since the suspending arms follow the movement of the manipulators satisfactory.

The model treated in this paper is a manipulator with two rigid links with two DOFs moving in vertical plane. It is shown that the tension of wires to suspend the manipulator with the rigid link must be controlled as constant value to simulate the microgravity condition and to demonstrate the dynamic behavior of a space robot. It is verified experimentally that using the present method it is possible to simulate the motion of the manipulator in space on the ground.

The present experimental system is expected to be used for simulation of the three-dimensional motion of a space robot and the dynamic behavior of the flexible manipulator.

References

[1]Umetani, Y., "Cosmo-Lab Project Proposed by Space Robotics Forum," *Proceedings of Space Artificial-Intelligence/Robotics/Automation Symposium* (Tokyo, Japan), 1989, pp. 44–46.

[2]Whittaker, W. L., Kanade, T., et al., "Space Robotics in Japan," Japanese Technology Evaluation Center, JTEC, Panel Rept., Jan. 1991.

[3]Longman, R. W., Lindberg, R. E., and Zedd, M. E., "Satellite-Mounted Robot Manipulators—New Kinematics and Reaction Moment Compensation," *International Journal of Robotics Research*, Vol. 6, No. 3, 1987, pp. 87–103.

[4]Longman, R. W., "Attitude Tumbling Due to Flexibility in Satellite Mounted Robots," *Proceedings of the AIAA Guidance, Navigation, and Control Conference* (Minneapolis, MN), AIAA, Washington, DC, 1988, pp. 365–373.

[5]Spofford, J., and Akin, D., "Redundancy Control of a Free-Flying Telerobot," *Proceedings of the AIAA Guidance, Navigation, and Control Conference* (Minneapolis, MN), AIAA, Washington, DC, 1988, pp. 347–357.

[6]Fujii, H., Takinami, M., and Uchiyama, M., "Mission Function Control for Flexible Arm of Robots Mounted on Space Structures," *Proceedings of the AIAA Guidance, Navigation, and Control Conference* (Boston, MA), AIAA, Washington, DC, 1989 (AIAA Paper 89-3566).

[7]Cannon, R. H., and Schmitz, E., "Initial Experiments on the End-Point Control of a Flexible One-Link Robot," *International Journal of Robotics Research*, Vol. 3, No. 3, 1984, pp. 62–75.

[8]Komatsu, T., Uenohara, M., Iikura, S., Miura, H., and Shimoyama, I., "Active Vibration Control for Flexible Space Environment Use Manipulators," *Proceedings of IUTAM/IFAC Symposium* (Zurich, Switzerland), 1988, pp. 49–60.

[9]Umetani, Y., and Yoshida, K., "Experimental Study on Two Dimensional Free-Flying Robot Satellite Model," *Proceedings of NASA Conference on Space Telerobotics*, 1989.

[10]Fujii, H., Uchiyama, K., and Sakemi, K., "Analysis of Space Manipulator System in Ground Simulation," *Proceedings of Space Artificial-Intelligence/Robotics/Automation Symposium* (Tokyo, Japan), 1989, pp. 122–125.

[11]Yoshida, K., "Control of the Space Robotic Manipulators," Ph.D. Dissertation, Tokyo Inst. of Technology, Tokyo, Japan, 1990 (in Japanese).

[12]Fujii, H., Uchiyama, K., Sugahara, K., and Uchiyama, T., "A Preliminary Study of Experimental Simulation on Dynamics of Space Manipulator System," *Proceedings of the AIAA Guidance, Navigation, and Control Conference* (Portland, OR), AIAA, Washington, DC, 1990, pp. 747–752.

[13]Matsunaga, S., and Natori, M., "On the Gravity Compensation of Space Structures by Suspension Wires," *Proceedings of 1990 Dynamics and Design (D & D) Conference* (Kawasaki, Japan), Vol. B, 1990, pp. 349–353 (in Japanese).

[14]Sato, Y., Ejiri, A., Iida, Y., Kanda, S., Maruyama, T., Uchiyama, T., and Fujii, H., "Micro-G Emulation System Using Constant Tension Suspension for a Space Manipulator," *Proceedings of the 1991 IEEE International Conference on Robotics and Automation* (Sacramento, CA), Inst. of Electrical and Electronics Engineers, 1991.

[15]Asada, H., Ma, Z.-D., and Tokumaru, H., "Inverse Dynamics of Flexible Robot Arms: Modeling and Computation for Trajectory Control," *Journal of Dynamic Systems, Measurement and Control*, Vol. 112, June 1990, pp. 177–185.

[16]Meirovitch, L., *Methods of Analytical Dynamics*, McGraw–Hill, New York, 1970, pp. 66–72.